International Journal of Engineering Technology and Management Sciences
Website: ijetms.in Issue: 6 Volume No.7 November - December – 2023
DOI:10.46647/ijetms.2023.v07i06.035 ISSN: 2581-4621

Metamaterial-inspired Antenna for LTE, BLUETOOTH and WiMAX Systems with Dual Band Capability

Mrs. Noorjahan.M[1], Ramesh.M[2], Mathiyazhagan.P[3], Gopikrishnan.G[4], Rajkumar.M[5]

[1]*Assistant Professor, Electronics & Communication Engineering, Dhanalakshmi Srinivasan Engineering College (Autonomous), Perambalur, Tamil Nadu.*
[2]*UG - Electronics & Communication Engineering, Dhanalakshmi Srinivasan Engineering College (Autonomous), Perambalur, Tamil Nadu.*
[3]*UG - Electronics & Communication Engineering, Dhanalakshmi Srinivasan Engineering College (Autonomous), Perambalur, Tamil Nadu.*
[4]*UG - Electronics & Communication Engineering, Dhanalakshmi Srinivasan Engineering College (Autonomous), Perambalur, Tamil Nadu.*
[5]*UG - Electronics & Communication Engineering, Dhanalakshmi Srinivasan Engineering College (Autonomous), Perambalur, Tamil Nadu.*
Corresponding Author Orcid ID: https://orchid.org//0009-0003-1984-4983

ABSTRACT
This study introduces a compact antenna, influenced by metamaterials, that functions across LTE, Bluetooth, and WiMAX frequency bands. The design employs an external square metallic strip for the lower band, causing the patch to emit a magnetic-current loop. An additional loop for the upper band is created by placing a metamaterial structure near the patch's feed line. The 42x32 mm^2 antenna is suitable for wireless devices. Its design and numerical analysis were conducted using the HFSS high-frequency structure simulator. A detailed mathematical derivation of the antenna's lumped circuit model is provided. The antenna operates in dual-band from 0.60 ~ 0.64GHz, 2.67 ~ 3.40GHz, and 3.61 ~ 3.67GHz, making it suitable for LTE and WiMAX applications. It also exhibits gains of 0.15 ~ 3.81 dBi and 3.47 ~ 3.75 dBi for the frequency ranges of 2.67 ~ 3.40GHz and 3.61 ~ 3.67GHz respectively.
Keywords – Metamaterials, HFSS high-frequency structure simulator, Dual-band

INTRODUCTION

Rapid advancements in wireless communication technologies have made lightweight, low-profile, high-performance, multi-band, low-frequency band antennas essential for supporting the growing number of service bands. Various communication systems operate in different frequency bands, including GSM-900, GSM-1800, GPS, WLAN at 2.4GHz and 5GHz, and LTE in lower, middle, and upper bands. ISPs and IEEE 802.11a devices use the U-NII spectrum, with different frequency ranges for low, mid, and high bands. WiMAX and Bluetooth operate in the 2.4–2.85GHz range in the ISM band, while ISPs use frequencies such as 2.3GHz, 2.5GHz, and 3.5GHz.Techniques to improve antenna performance. Metamaterial antennas utilize metamaterials to enhance the performance of miniaturized antenna systems and offer improved performance compared to traditional antennas. Advanced communication systems require metamaterials to improve bandwidth, gain, efficiency, and support lightweight, multi-band, and high data rate applications. Metamaterial antennas have the potential to be incorporated into future wireless communication systems due to their efficient and ideal performance. Metamaterials possess unique characteristics like negative permeability, double negative characteristics, and negative refractive index. Dual-band monopole antenna loaded with open complementary split-ring resonators (OCSRRs) covers the Bluetooth and WiMAX bands for

International Journal of Engineering Technology and Management Sciences
Website: ijetms.in Issue: 6 Volume No.7 November - December – 2023
DOI:10.46647/ijetms.2023.v07i06.035 ISSN: 2581-4621

improved performance. Antenna array with two 2x2 circularly polarized square slots (CPSS) is designed for the L- and S-band frequencies range of 1 to 4.34 GHz.

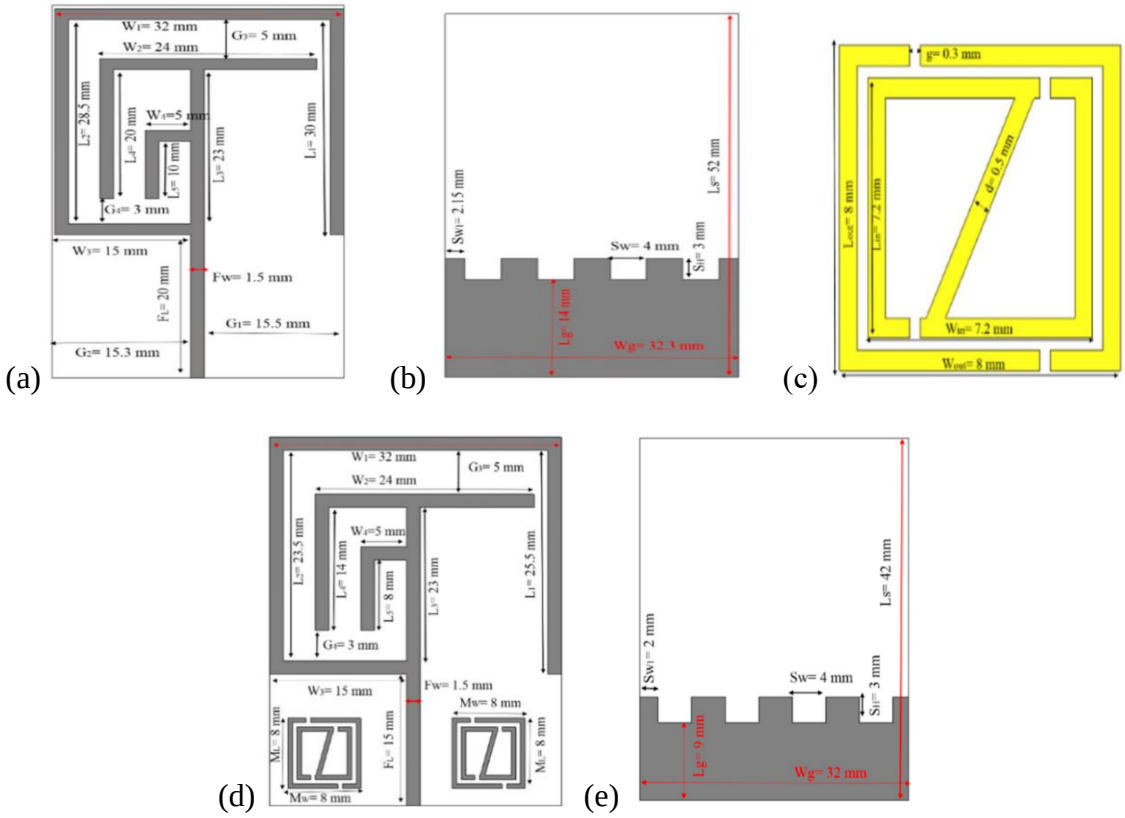

Figure 1. The geometry of the proposed: (a) Without MMs antenna front view, (b) Without MMs antenna back view, (c) Metamaterial (MMs) single unit cell, (d) With MMs antenna front view and (e) With MMs antenna back view.

The findings and discussion section analyzes the results of the study. It compares the performance of different antenna structures with and without metamaterials and faulty antenna ground planes. The section also explores the impact of integrating the metamaterial structure at different positions within the antenna construction. Additionally, it discusses the radiation pattern and current distribution of the antennas.

Methodology And Measurement

Based on a survey of the literature, Fig. 1(a–e) depicts the schematic geometries of a low profile, multifunctional, small sized, low frequency bands with and without metamaterial antenna. The three layers of the antennas are the ground plane, the antenna substrate, and the radiating patch. The antennas are designed in millimeter (mm) size. The 42x32mm² metamaterial antenna that is being exhibited is printed on a 1.60mm thick (t) FR-4 substrate that has a loss tangent of 0.02 and a relative permittivity of 4.50. There is a ground plane (12 x 32 mm2) with slots on the rear side of the object. Copper, with a conductivity of σ=5×8 s/m and a thickness of 0.035 mm, serves as both the antennas' ground plane and radiating patch. The feed line is 1.5mm width and there is a little change of the width of the feed line makes a significant change in the resonances of the antennas. The feeding metal strip is connected to a 50Ω mini coaxial cable for testing the antenna. the integrated metamaterial structure is composed by combining the two-ring resonator with an arrangement of splits and metal strips. A metal strips connected the upper and lower metal bar of the inner ring resonator and looks, like a ‘z-shape’ structure. While a single unit-cell dimension is set to 8.0×8.0×1.635 mm^3 along the respective (x, y, z) axes. All the designs, simulations and investigation are done through the computer simulation technology (HFSS) Microwave Studio electromagnetic simulator tool.

International Journal of Engineering Technology and Management Sciences
Website: ijetms.in Issue: 6 Volume No.7 November - December – 2023
DOI:10.46647/ijetms.2023.v07i06.035 ISSN: 2581-4621

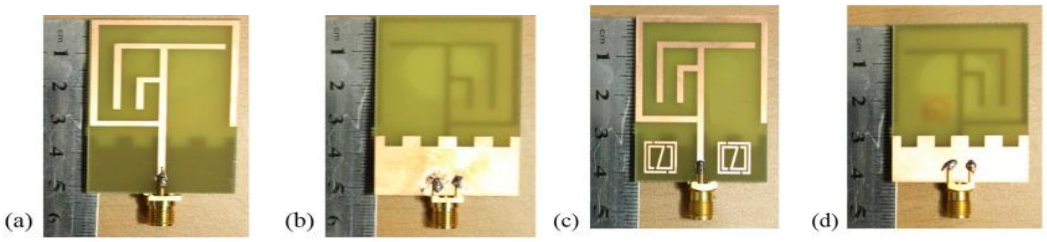

Figure 2. Fabricated geometry of the proposed: (a) Without MMs antenna front view, (b) Without MMs antenna back view, (c) With MMs antenna front view and (d) With MMs antenna back view.

Parameters	L_1	L_2	L_3	L_4	L_5	W_1	W_2	W_3	W_4
Size (mm)	25.5	23.5	23	14	8.0	32	24	15	5.0
Parameters	G_3	G_4	F_L	F_W	L_g	W_g	S_W	S_H	S_{W1}
Size (mm)	5.0	3.0	15	1.5	9.0	32	4.0	3.0	2.0

Table 1. Design specification of the proposed metamaterial (MMs) antenna

Design Equations for Metamaterial Antenna:

In addition, initially a patch is designed with a slotted ground for achieving low frequency resonance and then metamaterial are introduced to enhance the performances of the antenna with reduces of antenna size. However, the embedded metamaterial and slots in ground initial design equations are as follows.

$$M_W \approx M_L \approx \frac{L_S}{5.25} \approx \frac{W_S}{4} \quad (1)$$

$$S_H \approx \frac{L_g}{3} \approx \frac{W_g}{10.67} \approx \frac{S_w}{1.33} \quad (2)$$

where M_W and M_L are the length and width of the metamaterial unit cell in the patch, S_H is the length of slot, and S_W is the width of the slot in the ground plane. The dimensions of the designed metamaterial (MMs) unit cell are, outer resonator length (L_{out}) = 8.0 mm, outer resonator width (W_{out}) = 8.0 mm, inner resonator length (L_{IN}) = 7.20 mm, inner resonator width (W_{IN}) = 7.20mm, split gap (g) = 0.30mm and resonator metal strips width (d) = 0.5mm. Figure 2(a–d) illustrate the fabricated prototype of the proposed without metamaterial and with metamaterial integrated antennas. Moreover, Table 1 illustrates the design specification of the proposed MMs antenna. On the basis of fundamental theoretical equations, the mathematical formulae by which the design of proposed antenna was started can be derived as[21],

The Effective Dielectric Constant, $$\epsilon_{re} \approx \frac{\epsilon_r+1}{2} + \frac{\epsilon_r-1}{2}\left(1+\frac{12h}{w}\right)^{-0.5} \quad (3)$$

Fringing Length, $$\Delta L \approx 0.412\left\{\frac{(\epsilon_{re}+0.30)\left[\frac{w}{h}+0.26\right]}{\mathcal{L}\epsilon_{re}-0.258\left[\frac{w}{h}+0.80\right]}\right\}h \quad (4)$$

Fundamental Frequency, $$f_1 \approx \frac{C}{2(L+2\Delta L)\sqrt{\epsilon_{re}}} \quad (5)$$

Where ϵ_r is the dielectric constant of FR-4 substrate, ϵ_r =4.40, 'w' is the width of the antenna element and 'h' is the height of the substrate material. The length and width of the antenna element is given by,

Patch Length, $$L \approx \frac{\lambda_0}{2\sqrt{\epsilon_r}} - 2\Delta L \approx \frac{C_0}{2f_0\sqrt{\epsilon_r}} - 2\Delta L \quad (6)$$

Patch Width, $$w \approx \frac{\lambda_0}{z}\sqrt{\frac{\epsilon_r+1}{2}} \approx \frac{c_0}{2f_0}\sqrt{\frac{\epsilon_r+1}{2}} \quad (7)$$

To get a converged solution for the given design, it is necessary to properly choose the feeding mechanism, fine-tune the structure, apply the relevant electromagnetic boundary conditions, and—

International Journal of Engineering Technology and Management Sciences
Website: ijetms.in Issue: 6 Volume No.7 November - December – 2023
DOI:10.46647/ijetms.2023.v07i06.035 ISSN: 2581-4621

above all—choose the driving solution. The electromagnetic simulation program HFSS tool, which produces the finite integration technique of Maxwell's equations within boundary condition, has been used to investigate and numerically optimize the expected performances of the metamaterial embedded antenna in terms of return loss, gain, S-parameter, and radiation patterns. To analyze the characteristics of the proposed metamaterial structure for embedded in the antenna structure refection (S_{11}) and transmission (S_{21}) coefficients are extracted to calculate the effective permittivity (ε_r), permeability (μ_r), and refractive index (n_r) are expressed as follows[22,23],

$$V_1 = S_{21} + S_{11} \quad (8)$$

$$V_2 = S_{21} - S_{11} \quad (9)$$

$$\epsilon_r \approx \frac{2}{jk_0 d} \times \frac{(1 - V_1)}{(1 + V_1)}$$

Effective Permittivity, $\varepsilon_r \approx \frac{c}{j\pi f d} \times \left\{\frac{(1-S_{21}-S_{11})}{(1+S_{21}+S_{11})}\right\}$ (10)

$$\mu_r \approx \frac{2}{jk_0 d} \times \frac{(1 - V_2)}{(1 + V_2)}$$

Effective Permeability, $\mu_r \approx \frac{c}{j\pi f d} \times \left\{\frac{(1-S_{21}+S_{11})}{(1+S_{21}-S_{11})}\right\}$ (11)

$$n_r \approx \sqrt{\varepsilon_r \mu_r}$$

Refractive Index, $n_r \approx \frac{c}{j\pi f d} \times \sqrt{\left\{\frac{(S_{21}-1)^2 - S_{11}^2}{(S_{21}+1)^2 - S_{11}^2}\right\}}$ (12)

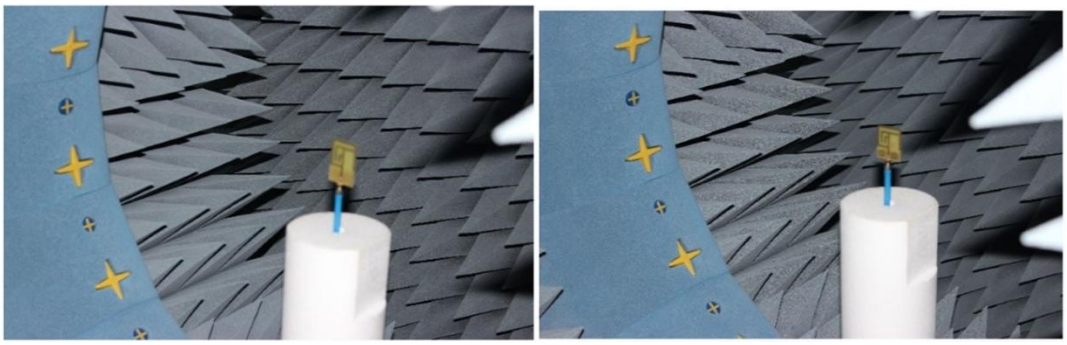

(a) (b)

Figure 4. Measurement in the Satimo StarLab: (**a**) Without MMs antenna and (**b**) With MMs antenna.

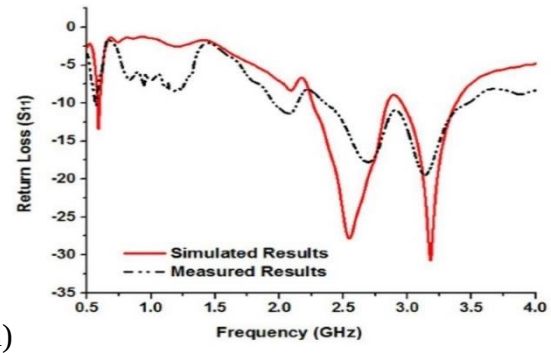

(a)

International Journal of Engineering Technology and Management Sciences
Website: ijetms.in Issue: 6 Volume No.7 November - December – 2023
DOI:10.46647/ijetms.2023.v07i06.035 ISSN: 2581-4621

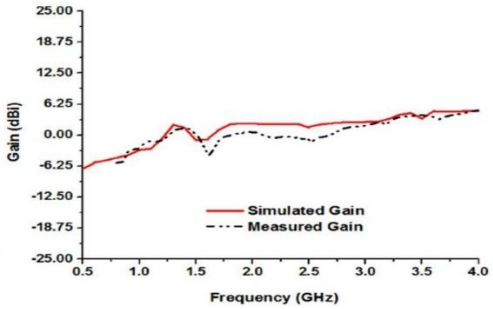

(b)

Figure 5. Measured and simulated: (**a**) Return loss (S_{11}) and (**b**) Gain of the without MMs antenna shown in Fig. 2(a,b).

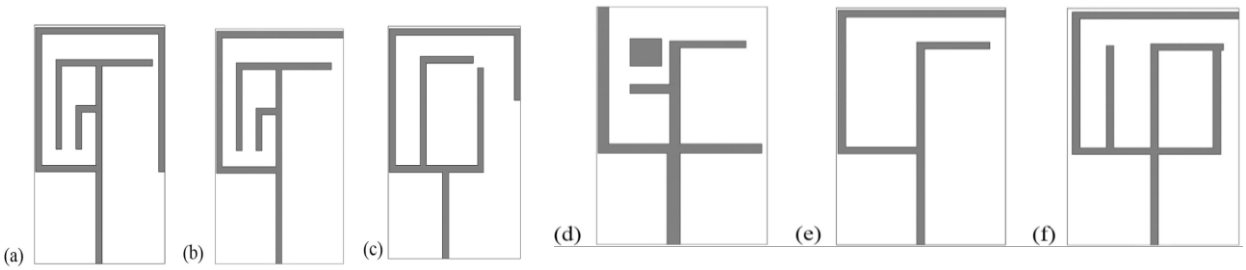

Figure 6. Parametric analysis of the designed different without MMs antenna geometry: (**a**) Antenna-1, (**b**) Antenna-2, (**c**) Antenna-3, (**d**) Antenna-4, (**e**) Antenna-5 and (**f**) Antenna-6

Validation and Measurement Results of Fabricated Antennas

To validate the simulation results, actual antennas without metamaterials and with metamaterials are fabricated on an epoxy resin fiber substrate. Measurements are performed using a vector network analyzer (VNA) and the Satimo StarLab near-field antenna measurement system. The results are compared to the simulated data.

Antenna Configurations	**Antenna-1**	**Antenna-2**	**Antenna-3**	**Antenna-4**	**Antenna-5**	**Antenna-6**
Resonant Frequency (GHz)	0.59, 2.55, 3.17	2.38, 2.73, 3.72	1.42,3.72	1.98, 3.36	0.91, 2.15, 3.83	0.90, 3.41
Band covered	L-, S-Band	S-Band	S-Band	L-, S-Band	L-, S-Band	L-, S-Band
Bandwidth (MHz)	30, 590, 430	220, 270, 710	40, 230	380, 680	40, 340, 350	30,1310
Efficiency	91%	94%	90%	97%	94%	93%

Table 2. Performances analysis of the designed antenna configurations

Fabrication and Scattering Parameter Measurements:

Antenna prototypes are fabricated on an epoxy resin fiber substrate. Scattering parameter and VSWR measurements are conducted using a VNA up to 20GHz. Slight discrepancies between the simulated and measured return loss are observed for the metamaterial antenna. The Satimo StarLab system is used for gain, efficiency, and radiation pattern measurements. The system employs a circular "arch" with 16 measuring probes for a full 3D scan of the antenna under test (AUT). Far-field data is used to calculate the gain and efficiency of the AUT.

Antenna without metamaterials:

Simulated resonance peaks at 0.59, 2.55, and 3.17GHz, with bandwidths of 30, 590, and 430MHz. Measured resonance peaks at 0.56, 2.67, and 3.15GHz, with bandwidths of 20MHz, 560MHz, and 580MHz.

International Journal of Engineering Technology and Management Sciences
Website: ijetms.in Issue: 6 Volume No.7 November - December – 2023
DOI:10.46647/ijetms.2023.v07i06.035 ISSN: 2581-4621

Antenna with metamaterials:

Measured gain ranges from 0.05 to 2.70 dBi (2.346 to 2.906GHz) and from 2.73 to 4.24 dBi (2.91 to 3.49GHz). Simulated gain ranges from 2.0 to 2.68 dBi (2.26 to 2.84GHz) and from 2.89 to 4.54 dBi (2.95 to 3.38 GHz). Frequency range: Measured gain frequency range is from 0.8GHz to 4.0GHz. Simulated frequency range is from 0.5GHz to 4.0GHz due to measurement capabilities.The measurement results provide validation for the simulated data, although slight discrepancies are observed.

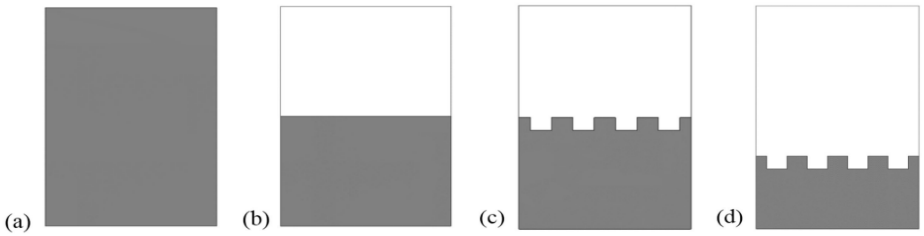

Figure 8. Parametric analysis of the without MMs antenna by: (a) Full ground plane, (b) Half ground plane, (c) Half slotted ground and (d) Slotted ground plane.

Numerical studies on antennas with different shapes, but without the embedded metamaterial structure, are shown in Figure 6(a-f). Figure 7(a, b) and Table 2 illustrate the changes in return loss (S11), bandwidth, and efficiency with different antenna structures. Antenna-1 exhibits three resonance points covering the L- and S-bands, with respective bandwidths of 30 MHz, 590 MHz, and 430 MHz. Antenna-5 also has three resonance peaks at 0.91 GHz, 2.15 GHz, and 3.83 GHz, but with smaller bandwidths compared to the antenna-1 configuration. The reduction of strip lines in the antenna-5 configuration leads to a shorter current path and a smaller metallic portion compared to the antenna-1 structure, resulting in variations between these two antenna configurations. It is observed that the high-frequency performance can be improved by employing a square metallic patch near the feed line (Figure 6(d)) and rearranging the metal bar in the antenna structure (Figure 6(b, c)).

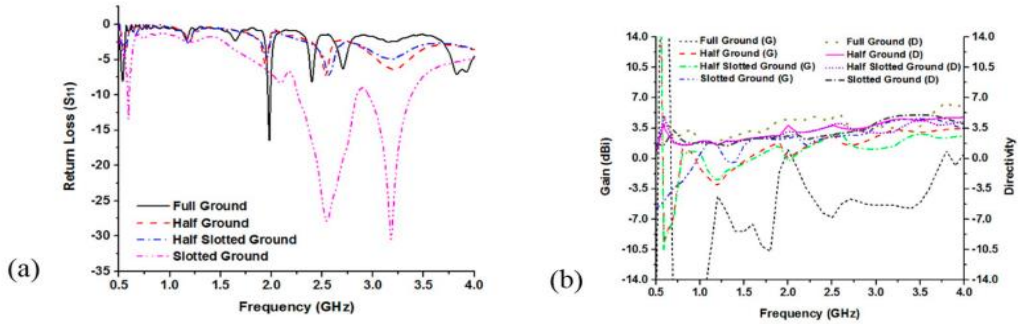

Figure 9. Performance analysis of the proposed without MMs antenna various ground plane structure by: (a) Return loss (S11) and (b) Gain & Directivity.

Transmittance Resonance	Permittivity	Permeability	Refractive Index
3.51 GHz	−17.24	−12.72	−15.07

Transmittance Resonance **Permittivity** **Permeability** **Refractive Index**

3.51 GHz −17.24 −12.72 −15.07

International Journal of Engineering Technology and Management Sciences
Website: ijetms.in Issue: 6 Volume No.7 November - December – 2023
DOI:10.46647/ijetms.2023.v07i06.035 ISSN: 2581-4621

Figure 10. (a) Scattering parameters and (b) Permittivity, permeability and refractive index of the embedded left-handed metamaterial structure results analysis of metamaterial antenna.

The metamaterial's electromagnetic properties are shown in Fig. 10(a) and (b). Transmittance resonance at 3.18 GHz and reflectance at 3.55 GHz are observed. Negative permeability is achieved from 2.21 to 4.0GHz, and negative permittivity at two frequency ranges: 1.59 to 2.96GHz and 3.38 to 3.83GHz. The refractive index shows two major negative frequency ranges: 1.63 to 3.06GHz and 3.09 to 3.85GHz. If permittivity and permeability are both negative, the refractive index will be negative, which occurs in the frequency ranges of 2.21 to 2.97GHz and 3.38 to 3.84GHz, making the structure a left-handed metamaterial at these frequencies. At the transmittance resonance point of 3.51GHz, the permittivity, permeability, and refractive index are -17.24, -12.72, and -15.07 respectively (Table 3). The simulated results of the proposed antenna show resonance points at 0.65GHz, 3.18GHz, and 3.51GHz with operating bands over specific frequency ranges, while the measured results show resonance points at 0.63GHz, 3.21GHz, and 3.63GHz with slightly different bandwidths.

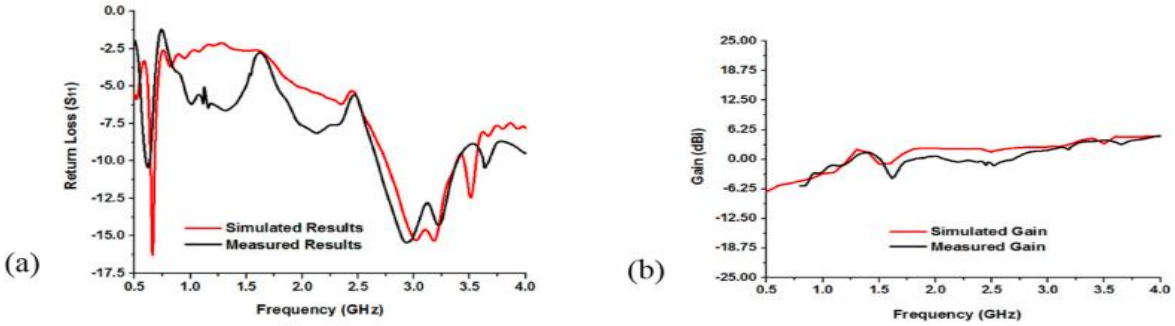

Figure 11. Measured and simulated: (a) Return loss (S11) and (b) Gain of the metamaterial embedded antenna shown in Fig. 2(c,d).

The substrate's relative permittivity affects the difference between simulated and measured results. A higher permittivity shifts the resonant frequency to a lower frequency. The measured gains at the two operating frequency bands are 0.153.81 dBi and 3.473.75 dBi over 2.673.40 GHz and 3.613.67 GHz, respectively (as shown in Fig. 11(b)). The measured gain frequencies range from 0.8 GHz to 4.0 GHz, while the simulated frequencies range from 0.5 GHz to 4.0 GHz due to the measurement capabilities of Satimo StarLab (Fig. 11(b)). The antenna structure shown in Figure 12(a-d) includes embedded metamaterial. Metamaterial is an artificial material with unique electromagnetic properties. The different configurations of the metamaterial-embedded antenna cover the L- and S-bands with variations in resonant points and bandwidths. Bandwidth is an important parameter indicating how well an antenna can radiate or receive energy across a range of frequencies.

International Journal of Engineering Technology and Management Sciences
Website: ijetms.in Issue: 6 Volume No.7 November - December – 2023
DOI:10.46647/ijetms.2023.v07i06.035 ISSN: 2581-4621

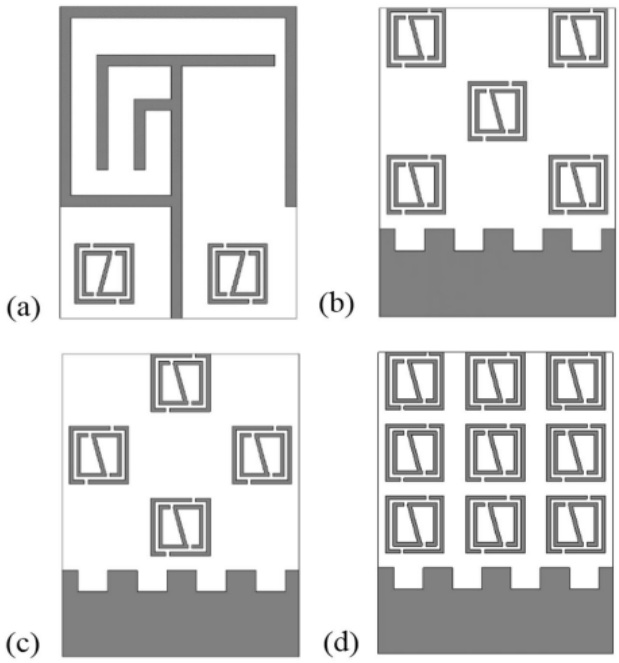

Figure 12. Metamaterial integration at various position of the proposed MMs antenna: (a) MMs antenna conf.- 1, (b) MMs antenna conf.-2, (c) MMs antenna conf.-3 and (d) MMs antenna conf.-4

MMs Antenna Configurations	Resonant Frequency	Band Covered	Bandwidths
MMS Antenna Conf.-1	0.65 GHz, 3.18 GHz, 3.51 GHz	L-, S-Band	44 MHz, 630 MHz, 110 MHz
MMS Antenna Conf.-2	0.59 GHz, 2.89 GHz, 3.59 GHz	L-, S-Band	36 MHz, 330 MHz, 267 MHz
MMS Antenna Conf.-3	0.60 GHz, 2.92 GHz, 3.58 GHz	L-, S-Band	32 MHz, 431 MHz, 280 MHz
MMS Antenna Conf.-4	0.56 GHz, 2.76 GHz, 3.83 GHz	L-, S-Band	15 MHz, 185 MHz, 773 MHz

Table 4. Performances of the proposed MMs antenna at different configurations.

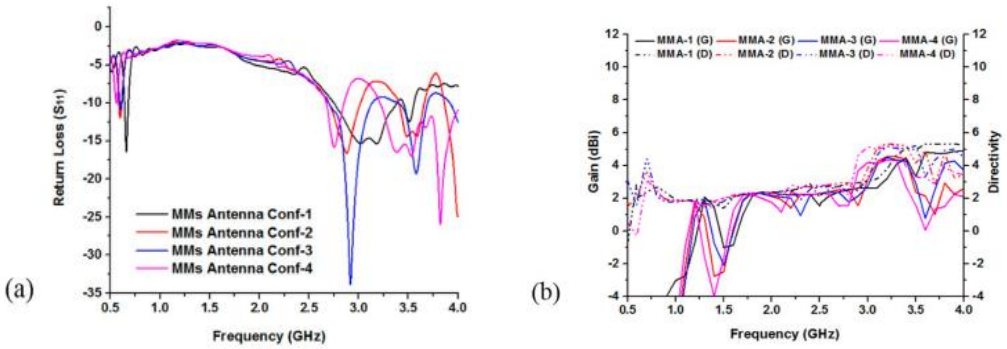

Figure 13. Performance analysis by integration MMs at different position of the proposed metamaterial antenna: (a) Return loss (S11) and (b) Gain & Directivity.

International Journal of Engineering Technology and Management Sciences
Website: ijetms.in Issue: 6 Volume No.7 November - December – 2023
DOI:10.46647/ijetms.2023.v07i06.035 ISSN: 2581-4621

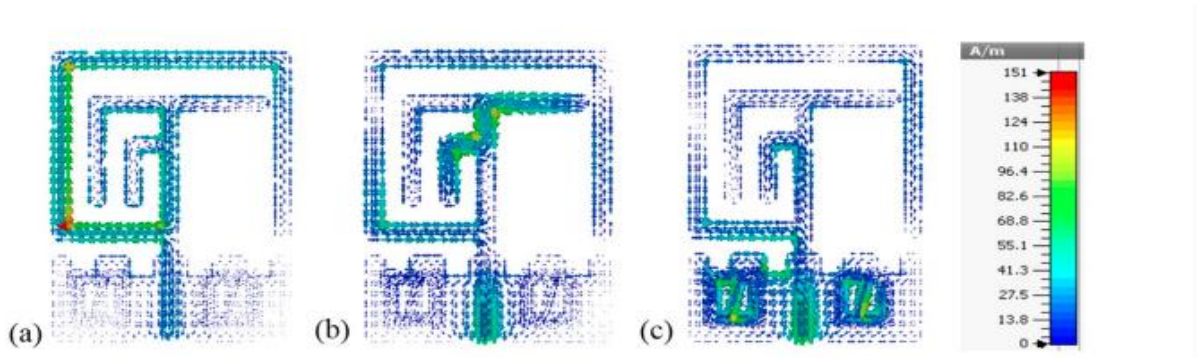

Figure 14. Surface Current distribution of the proposed MMs antenna at, (a) 0.63GHz, (b) 3.21GHz and (c) 3.63GHz

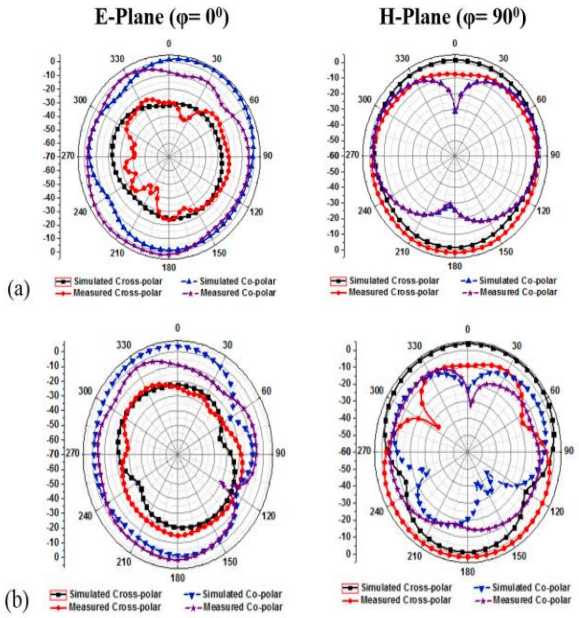

Figure 15. Simulated and Measured radiation pattern of proposed metamaterial inspired antenna at: (a) 3.21GHz and (b) 3.63GHz.

Figure 15: (a,b) show the comparison between measured and simulated far-field radiation patterns in E-plane and H-plane. The figures are shown from the relevant pattern from ϕ=0° (E-plane) and ϕ=90° (H-plane).

References	Antenna Dimension	Resonant Frequency (GHz)	Covered Bands	Bandwidth (MHz)	Gain (dBi)	Applications
Martínez *et al.*[3]	40 × 30 mm^2	2.40, 3.60	S-Band	230, 220	1.4, 1.7	Bluetooth, WiMAX
Li *et al.*[5]	45 × 50 mm^2	2.25	S-Band	330	0.97	Bluetooth
Huang *et al.*[6]	45 × 40 mm^2	2.40, 5.20	S- and C-Band	1300, 1800	3.20, 2.34	WLAN, WiMAX
Bakariya *et al.*[7]	27 × 24 mm^2	2.40, 3.50, 5.70	S- and C-Band	85, 400, 125	1.3, 2.5, 3.8	Bluetooth, WLAN, WiMAX

DOI:10.46647/ijetms.2023.v07i06.035 ISSN: 2581-4621

Pushpakaran *et al.*[8]	40 × 38 mm^2	2.47, 5.18	S- and C-Band	310, 560	4.5, 7.0	WLAN
Cao *et al.*[10]	44 × 56 mm^2	1.54, 2.41, 3.25	L- and S-Band	90, 145, 700	−2, 1.52, 3.0	GPS, WLAN, WiMAX
Zhang *et al.*[14]	115 × 42 mm^2	0.90, 1.88	L- and S-Band	376, 1757	0.8, 2.05	GSM
Liu *et al.*[15]	115 × 60 mm^2	0.85, 1.75	L- and S-Band	271, 1125	2.5, 3.37	GSM, WLAN
Abed *et al.*[16]	70 × 50 mm^2	2.45, 3.60	S-Band	260, 350	—	WiFi, WiMAX
Nandi *et al.*[17]	45 × 25 mm^2	2.40, 3.50	S-Band	270, 150	−2.0, 0.14	WLAN, WiMAX
Trong *et al.*[18]	88 × 88 mm^2	0.9, 1.70	L- and S-Band	40, 120	−0.7, 4.5	GSM
Lee *et al.*[19]	220 × 320 mm^2	2.40, 5.20	S- and C-Band	84, 200	6.9, 6.8	WLAN
Chen *et al.*[20]	140 × 75 mm^2	0.95	L-Band	262	—	LTE
Proposed MMs Antenna	42 × 32 mm^2	0.63, 3.21, 3.63	L- and S-Band	40, 730, 60	3.0, 3.69	LTE, WiMAX

Table 5. Performance comparison between the proposed MMs antenna with the existing antenna

The content discusses different antennas with varying structures, dimensions, substrate materials, and ground plane designs. These antennas exhibit identical resonant frequencies but differ in terms of bandwidth, gain, and applications.

After a detailed investigation of the existing antennas in Table 5, it is concluded that the proposed metamaterial inspired antenna is compact in size, covers lower frequency bands, has moderate gain, larger bandwidths, and is applicable for LTE and WiMAX applications.

Conclusion

Advancements of wireless communications and electronic warfare systems in new cutting-edge technologies, include metamaterial antennas for leading the improvements in overall system performance. To adjust with the modern wireless communication systems, a metamaterial inspired antenna with covering the L- and S-band frequencies is designed, analyzed and measured in this paper. Simulation results show the metamaterial inspired antenna works well in the lower (0.645~0.689 GHz) and upper (2.75~3.38 GHz) as well as (3.45~3.56 GHz) frequency range. Experimental results are very close to the simulation ones, where the covered lower and upper bands are respectively, (0.60~0.64 GHz), (2.67~3.40 GHz), (3.61~3.67 GHz). The antenna exhibits Omni-directional radiation pattern during the operating frequency band with the high peak gain. the antenna can be fabricated easily as well as cheap, simple, and compact for small portable devices. Moreover, The proposed without MMs antenna and with MMs antenna have stable radiation characteristics, high efficiency, low back lobe and good candidate for LTE, Bluetooth, WiMAX, etc. applications.

References

1. Hasan, M. M., Faruque, M. R. I., Islam, S. S. & Islam, M. T. A New Compact Double-Negative Miniaturized Metamaterial for
Wideband Operation. Materials 9(10), 830 (2016).
2. Hasan, M. M., Faruque, M. R. I. & Islam, M. T. Inverse E-Shape Chiral Metamaterial for Long Distance Telecommunication. Microw. Opt. Technol. Lett. 59, 1772–1776 (2017).

DOI:10.46647/ijetms.2023.v07i06.035 ISSN: 2581-4621

3. Martínez, F. J., Zamora, G., Paredes, F., Martín, F. & Bonache, J. Multiband printed monopole antennas loaded with OCSRRs for
PANs and WLANs. IEEE Antennas Wirel. Propag. Lett. 10, 1528–1531 (2011).
4. Pourahmadazar, J. & Rafii, V. Broad Biand circularly polarised slot antenna array for L- and S-band applications. Electron. Lett.
48(10), 542–543 (2012).
5. Li, T., Zhai, H., Wang, X., Li, L. & Liang, C. Frequency-Reconfigurable Bow-Tie Antenna for Bluetooth, WiMAX, and WLAN Applications. IEEE Antennas Wirel. Propag. Lett. 14, 171–174 (2015).
6. Huang, H., Liu, Y., Zhang, S. & Gong, S. Multiband Metamaterial-loaded Monopole Antenna for WLAN/WiMAX Applications.
IEEE Antennas Wirel. Propag. Lett. 14, 662–665 (2014).
7. Bakariya, P. S., Dwari, S., Sarkar, M. & Mandal, M. K. Proximity Coupled Microstrip Antenna for Bluetooth, WiMAX and WLAN Applications. IEEE Antennas Wirel. Propag. Lett. 14, 755–758 (2014).
8. Pushpakaran, S. V. et al. A Metaresonator Inspired Dual Band Antenna for Wireless Applications. IEEE Trans. Antennas Propag.
62(4), 2287–2291 (2014).
9. Wong, K. L. & Chen, L. Y. Small-Size LTE/WWAN Tablet Device Antenna with Two Hybrid Feeds. IEEE Trans. Antennas Propag.
62(6), 2926–2934 (2014).
10. Cao, Y. F., Cheung, S. W. & Yuk, T. I. A Multi-band Slot Antenna for GPS/WiMAX/WLAN Systems. IEEE Trans. Antennas Propag.
63(3), 952–958 (2015).
11. Shuai, C. Y. & Wang, G. M. A Novel Planar Printed Dual-Band Magneto-Electric Dipole Antenna. IEEE Access 5, 10062–10067 (2017).
12. Chou, Y. J., Lin, G. S., Chen, J. F., Chen, L. S. & Houng, M. P. Design of GSM/LTE multiband application for mobile phone antennas.
Electron. Lett. 51(17), 1304–1306 (2015).
13. Deng, C., Lv, X. & Feng, Z. High Gain Monopole Antenna with Sleeve Ground Plane for WLAN Applications. IEEE Antennas Wirel.
Propag. Lett. 16, 2199–2202 (2017).
14. Zhang, T., Li, R. L., Jin, G. P., Wei, G. & Tentzeris, M. M. A Novel Multiband Planar Antenna for GSM/UMTS/LTE/Zigbee/RFID Mobile Devices. IEEE Trans. Antennas Propag. 59(11), 4209–4213 (2011).
15. Liu, H. J. et al. A Multi-Broad Biand Planar Antenna for GSM/ UMTS/LTE and WLAN/WiMAX Handsets. IEEE Trans. Antennas
Propag. 62(5), 2856–2860 (2014).
16. Abed, A. T. & Singh, M. S. J. Slot antenna single layer fed by step impedance strip line for Wi-Fi and Wi-Max applications. Electron.
Lett. 52(14), 1196–1198 (2016).
17. Nandi, S. & Mohan, A. CRLH unit cell loaded tri-band compact MIMO antenna for WLAN/WiMAX applications. IEEE Antennas
Wirel. Propag. Lett. 16, 1816–1819 (2017).
18. Trong, N. N., Piotrowski, A. & Fumeaux, C. A Frequency-Reconfigurable Dual-Band Low-Profile Mono polar Antenna. IEEE Trans.
Antennas Propag. 65(7), 3336–3343 (2017).
19. Lee, C. T., Su, S. W., Chen, S. C. & Fu, C. S. Low-Cost, Direct-Fed Slot Antenna Built in Metal Cover of Notebook Computer for
2.4/5.2/5.8-GHz WLAN Operation. IEEE Trans. Antennas Propag. 65(5), 2677–2682 (2017).

DOI:10.46647/ijetms.2023.v07i06.035 ISSN: 2581-4621

20. Chen, H. D., Yang, H. W. & Sim, C. Y. D. Single Open-Slot Antenna for LTE/WWAN Smartphone Application. IEEE Trans. Antennas
Propag. 65(8), 4278–4282 (2017).
21. Balanis, C. A. Antenna Theory: Analysis and Design. 3rd Edition. Hoboken. NJ, USA: John Wiley & Sons, Inc. 816–826 (2005).
22. Hasan, M. M., Faruque, M. R. I. & Islam, M. T. Compact Left-Handed Meta-Atom for S-, C- and Ku-Band Application. Appl. Sci.
7(1071), 1–20 (2017).
23. Luukkonen, O., Maslovski, S. I. & Tretyakov, S. A. A stepwise Nicolson–Ross–Weir based material parameter extraction method.
IEEE Antennas Wirel. Propag. Lett. 10, 1295–1298 (2011).
24. Clayton, R. P. Inductance: Loop and Partial, New York, NY, USA: Wiley (2009).
25. Hasan, M. M., Faruque, M. R. I. & Islam, M. T. A Mirror Shape Chiral Meta Atom for C-Band Communication. IEEE Access 5,
21217–21222 (2017).